AIAA JOURNAL
Vol. 49, No. 10, October 2011

Plasma Flow Control of Cylinders in a Tandem Configuration

Alexey V. Kozlov* and Flint O. Thomas†
University of Notre Dame, Notre Dame, Indiana 46530

DOI: 10.2514/1.J050976

The tandem cylinder in crossflow represents a canonical flowfield geometry that is relevant to the landing gear noise generation process. In this paper, active flow control in the form of dielectric barrier discharge plasma actuation on the upstream cylinder is used to control the tandem cylinder flowfield with the objective of reducing unsteady pressure fluctuations on the downstream cylinder. Two types of plasma actuators are applied to the upstream cylinder. These include spanwise-oriented plasma actuators and plasma streamwise vortex generators. Flow control experiments were performed over the Reynolds number range $22,000 \le Re_D \le 172,000$, and the results obtained at both the lowest and highest Reynolds numbers are reported in this paper. In each case, baseline flowfield measurements are compared with those using plasma flow control. Results include global flow visualization, unsteady pressure measurements on the downstream cylinder, and nonintrusive near-wake surveys using laser Doppler velocimetry. It is demonstrated that both methods of plasma flow control lead to a more benign wake interaction with the downstream cylinder, which dramatically reduces surface pressure fluctuations.

Nomenclature

C_p	=	pressure coefficient
D	=	cylinder diameter
f_s	=	vortex shedding frequency
L	=	cylinder center-to-center streamwise separation distance
ℓ	=	spatial extent of separated flow region
P_s	=	surface pressure
P_∞	=	freestream static pressure
R	=	cylinder radius
Re_D	=	Reynolds number (based on freestream velocity and cylinder diameter)
St_D	=	Strouhal number (based on freestream velocity and cylinder diameter)
U_∞	=	freestream speed
u	=	streamwise-component velocity fluctuation
v	=	cross-stream component velocity fluctuation
x	=	streamwise spatial coordinate
y	=	cross-stream spatial coordinate
z	=	plasma streamwise vortex generator spanwise electrode spacing
θ	=	azimuthal angle on the cylinder

I. Introduction

A PRIMARY source of airframe noise for commercial transport aircraft on landing approach is the landing gear. The separated flow over the undercarriage is inherently unsteady and is characterized by multiple wakes that interact with downstream gear components, thereby providing sources of broadband noise. The tandem circular cylinder in crossflow is a simpler canonical bluff-body flow geometry that nonetheless reproduces many of the essential aspects of the landing gear noise generation process. Of particular interest is the nature of the interaction of the unsteady wake from the upstream cylinder with the downstream cylinder. In addition to the Reynolds number, the character of this interaction depends on the (center-to-center) cylinder streamwise separation L, in relation to the diameter D, of the two cylinders. Because of its relevance to landing gear noise generation mechanism(s), the tandem cylinder configuration has received considerable attention in both recent experimental studies [1–6] as well as numerical simulations [6–10]. Indeed, the tandem cylinder in crossflow has been designated a benchmark aeroacoustic flow by NASA.

A comprehensive review of the flow around two circular cylinders of the same diameter in tandem arrangement at subcritical Reynolds number was given by Zdravkovich [11]. It was shown that, for $2.5 < L/D < 3.2$, intermittent vortex shedding occurs in the gap region between the cylinders, whereas constant vortex shedding occurs only behind the downstream cylinder. Although occasionally one of the reattachments on the forward face of the rear cylinder is disrupted, there is no regular vortex shedding behind the front cylinder. For $3.2 < L/D < 3.8$, the flow between the cylinders is bistable and exhibits mode switching between intermittent and steady shedding from the front cylinder. Constant vortex shedding occurs only from the rear cylinder. For $L/D > 3.8$, constant vortex shedding occurs from both cylinders. The fluctuating pressure on circular cylinders in a tandem configuration was measured by Arie et al. [12] in the upper subcritical regime. They found the rms lift and drag was much larger on the downstream cylinder for $L/D < 7$. They became virtually identical for $L/D > 10$. This provides an effective upper bound on L/D for significant wake interaction.

For tandem cylinders at supercritical Reynolds numbers, the flow behavior also varies with cylinder spacing L/D, as is nicely summarized in Fig. 5 of the paper by Gu [13].

Motivated by the need for landing gear noise reduction, active flow control experiments on single cylinders in crossflow using single dielectric barrier discharge (DBD) plasma actuators have been performed [14–17]. These proof-of-concept studies using the "plasma fairing" concept have demonstrated the ability of DBD plasma actuators to eliminate unsteady von Kármán vortex shedding from cylinders at subcritical Reynolds numbers, significantly reduce turbulence levels in the wake, and reduce aerodynamic noise in a frequency band centered on the shedding frequency. Large-eddy simulation of the cylinder plasma flow control experiment reported in [15] was performed by Kim and Wang [18]. In their paper, the effect of the plasma was modeled as a body force in the governing equations. Good agreement between the simulations and experiment were reported for both quasi-steady and pulsed-plasma actuation. This study showed that large-scale vortex shedding is virtually eliminated by both steady and unsteady actuation and that the mean drag as well as drag and lift fluctuations are significantly reduced. The frequency of unsteady actuation was found to have a large effect on the control performance, with the Strouhal number range $1 \le St_D \le 1.5$ giving optimum results.

Presented as Paper 2010-4703 at the Fifth AIAA Flow Control Conference, Chicago, IL, 28 June–1 July 2010; received 5 October 2010; revision received 7 April 2011; accepted for publication 11 April 2011.

*Postdoctoral Research Associate, Department of Aerospace and Mechanical Engineering.

†Professor, Department of Aerospace and Mechanical Engineering. Associate Fellow AIAA.

For a comprehensive review of flow control applications of DBD plasma actuators, the reader is referred to Corke et al. [19] and Moreau [20].

In this paper, DBD plasma flow control is applied to a tandem cylinder configuration for the first time, in an effort to control the interaction between the upstream cylinder wake and downstream cylinder. Flow control takes the form of two types of surface-mounted DBD plasma actuators on the upstream cylinder. Because radiated noise is directly related to the unsteady force on the downstream cylinder [21], the upstream cylinder wake is manipulated in such a manner so as to reduce the unsteady surface pressure fluctuations on the downstream cylinder. To avoid ambiguities associated with bimodal behavior as reported in [11], the center-to-center separation L between the twin cylinders of diameter D is fixed at $L/D = 4$, which is just outside of the intermittent shedding region and for which vortex shedding from both cylinders occur. The Reynolds number for the flow control experiments varies over the subcritical range $22,000 \leq Re_D \leq 172,000$.

II. Description of the Experiment

The flow control experiments are performed in one of the low-turbulence, subsonic, in-draft wind tunnels located at the Hessert Laboratory for Aerospace Research at the University of Notre Dame. The wind tunnel has an inlet contraction ratio of 20:1. A series of 12 turbulence management screens at the front of the inlet gives rise to tunnel freestream turbulence levels less than 0.1% (and less than 0.06% for frequencies above 10 Hz). Experiments are performed in a test section of 0.610 m square cross section 1.82 m in length. One sidewall and the ceiling have optical access for both flow visualization and nonintrusive laser flowfield diagnostics [laser Doppler anemometry (LDA)].

The tandem configuration used in the current study is represented by two circular cylinder models of nominally the same diameter D, which are mounted in the wind-tunnel test section as shown schematically in Fig. 1. Two different circular cylinder models, each equipped with a different type of DBD plasma actuation, were used as the upstream cylinder of the tandem configuration. These are shown schematically in Figs. 1–3. One of the cylinder models is equipped with two spanwise-oriented plasma actuators, as shown in Fig. 2. The other has 15 streamwise oriented actuators [so-called plasma streamwise vortex generators (PSVG)], shown in Fig. 3. Both upstream cylinder models are formed from identical quartz glass cylinders (Fig. 3c, no. 1) with an outer diameter $D = 65$ mm, wall thickness $d = 2.5$ mm, span of 533.4 mm, and dielectric constant of

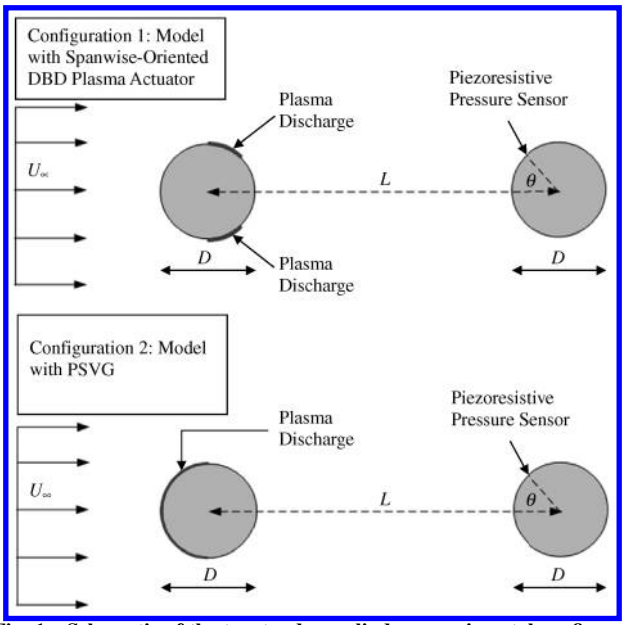

Fig. 1 Schematic of the two tandem cylinder experimental configurations.

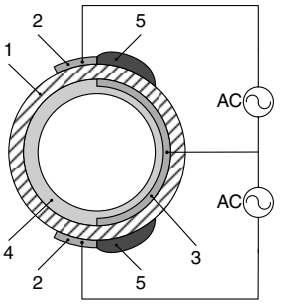

Fig. 2 Upstream cylinder model equipped with twin spanwise-oriented plasma actuators.

3.7. In both the configurations shown in Figs. 2 and 3, the cylinder wall serves as the dielectric barrier for the DBD plasma actuator. The ends of both cylinders terminate in plastic endplates, which elongate the models by 9.5 mm.

For the cylinder model with twin spanwise actuators (see Fig. 2), the covered electrodes are common for both plasma actuators due to space limitations. As indicated, the outer, exposed electrode (Fig. 2, no. 2) is mounted to the surface of the cylinder with its plasma generating edges located at $\pm 90°$ with respect to the approach flow direction. This choice for the electrode positioning is based upon the idea that the best location for the plasma actuators is near the separation point. Both covered and exposed electrodes are made of Saint Gobain C661 1.6-mil (0.041-mm)-thick copper foil tape with acrylic adhesive. The foil thickness is small compared with the local boundary-layer thickness so that the presence of the exposed electrodes does not change the flow significantly. The covered electrode (Fig. 2, no. 3) is mounted to the inner surface of the cylinder. Both inner and outer electrodes extend 0.457 m in the spanwise direction, which is equal to 83% of the total span of the model.

For both actuators, eight layers of 5-mil-thick Kapton tape (Fig. 2, no. 4) cover the inner electrodes and serve to prevent inner discharge. The inner and outer electrodes for the spanwise actuator have a small overlap, which gives rise to a large local electric field gradient. Plasma discharge (Fig. 2, no. 5) forms near the edge of the exposed electrodes and extends a distance along the cylinder's dielectric surface, as depicted in Fig. 2. As indicated in the figure, the actuators are connected to a high-voltage ac source.

For the upstream cylinder model equipped with PSVG, another configuration of electrodes is used as shown in Fig. 3. A schematic illustration of the PSVG concept on a flat plate is shown in Fig. 3a. The multiple exposed electrodes with spanwise spacing z are aligned parallel to the oncoming flow direction. The covered electrode is now common for all exposed electrodes, so the plasma discharge ignites at both edges of each exposed electrode. This arrangement creates opposing spanwise-oriented wall jets that collide between adjacent electrodes and give rise to pairs of counter-rotating streamwise vortices. In the cylinder application, which is illustrated in Fig. 3b, these will introduce streamwise vorticity into the nascent wake shear layers, thereby reducing large-scale spanwise vortex shedding [17]. As shown in Fig. 3b, the cylinder model has 15 exposed streamwise oriented electrodes of 0.25 in. (6.35 mm) in width with a spanwise spacing of $z = 1.25$ in. (31.75 mm). The PSVG actuators cover the windward half of the cylinder (from -90 to $+90°$), as shown schematically in Fig. 3c. The ends of the exposed electrodes are tied together at the rear side of the model. The covered electrode is similar to the one used for the spanwise model, but it is located under the windward half of the cylinder. It is noted that the spanwise electrode spacing used in the experiments reported here was not based upon a preferred hydrodynamic length scale. Rather, based on the boundary-layer flow control results of Schatzman and Thomas [22], $z = 1.25$ in. represented an optimum spacing in terms of effective production of streamwise vorticity for the range of applied voltages used in this study.

In this study, the spanwise actuator uses a positive sawtooth waveform ac voltage of 55 kV peak-to-peak at 1 kHz. The

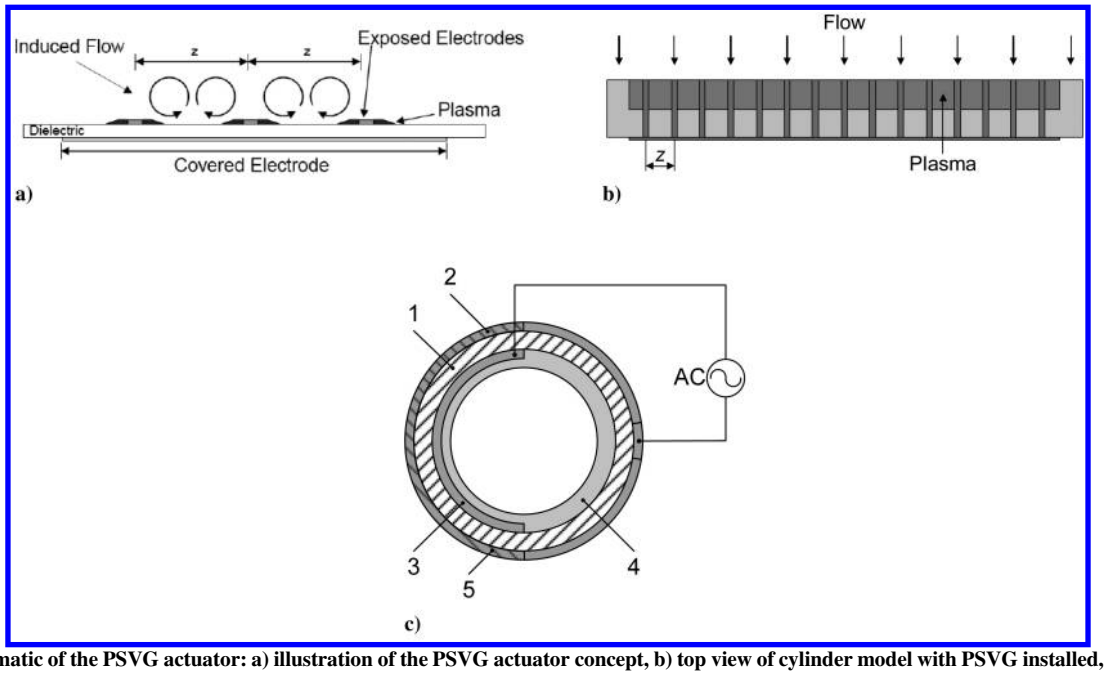

Fig. 3 Schematic of the PSVG actuator: a) illustration of the PSVG actuator concept, b) top view of cylinder model with PSVG installed, and c) cross-sectional view of cylinder showing a single streamwise oriented actuator.

streamwise oriented actuators use a sinusoidal ac voltage of 69 kV peak-to-peak at 500 Hz. Whereas the sawtooth waveform has been shown to give a higher body force [23], the sinusoidal waveform at lower frequency was chosen for the PSVG in order to reduce the load on the power amplifier because of the high total electric capacitance of the series of 15 streamwise actuators. The high voltage is measured with a LeCroy PPE20kV dc high-voltage probe in conjunction with a LeCroy LT262 oscilloscope. These ac voltage amplitudes were held constant for the entire Reynolds number range investigated in the flow control experiments. That is, no attempt was made to increase actuator authority with increase in Reynolds number.

The downstream cylinder of the tandem configuration is not instrumented with plasma actuators and is placed downstream of the first cylinder with the line of separation between centers of the two cylinders aligned with the wind-tunnel approach flow. The distance between the axes of the two cylinders was fixed at $L = 260$ mm ($L/D = 4$). This cylinder is made of polycarbonate pipe with outer diameter of 2.5 in. (63.5 mm) and inner diameter of 2 in. (50.8 mm). The length of the second cylinder is 550 mm. To measure the fluctuating surface pressure distribution as a function of angular position θ (as defined in Fig. 1) with a single transducer, one end of the cylinder is attached to the shaft of a stepper motor installed on the tunnel test section wall. The motor has 48 steps per revolution, resulting in the rotation of the model with a $\Delta\theta = 7.5°$ increment. The other end of the cylinder is connected to the wall of the test section with a plastic bearing. The unsteady surface pressure is measured with a flush surface-mounted Endevco model 8507C-1 miniature differential piezoresistive pressure sensor with 1 psi (6895 Pa) pressure range. The pressure transducer has a diameter of 2.34 mm and was positioned at the midspan location on the downstream cylinder. The surface pressure is measured relative to the static pressure in the uniform flow approximately $2.5D$ in front of the upstream cylinder model. The sensor signal is conditioned by a dc amplifier (Endevco model 136) and acquired by a personal computer using a Microstar iDSC 1816 A/D board. This board has onboard fourth-order analog antialiasing filters. The signal from the pressure transducer was sampled at 12.8 kHz and antialias filtered at 5632 Hz. Measurements of both the mean and unsteady rms surface pressure distributions on the downstream cylinder were performed for both natural and plasma control cases.

Flow visualization images were obtained using a TSI particle image velocimetry CAM 10-30 digital camera in conjunction with a Y120-15 New Wave Research Nd:Yag laser. Continuous olive oil fog consisting of 1-μ-diam droplets generated by a Dantec particle seeder were introduced upstream of the wind-tunnel inlet contraction. The Nd:Yag laser was used to illuminate the fog in the spanwise centerplane of the wind-tunnel test section.

Nonintrusive near-wake velocity measurements between the two cylinders were conducted using a Dantec Dynamics LDA system with fiber flow optical system, BSA-F60 flow processor, BSA flow software version 4.40.02, and Spectra-Physics stabilite 2017 argon-ion laser. The fiber optic LDA system was operated in the 180° backscatter mode. The optical configuration produced a probe volume of dimension 0.2 mm in both the streamwise and cross-stream directions. This defines the effective spatial resolution for the LDA measurements. To position the fiber optic head, a three-component stepper motor traverse system with Aerotech Unidex11 motion controller is used. The same 1-μ-diam olive oil droplets used for flow visualization were used as laser Doppler velocimetry (LDV) seed particles. At 95% confidence, the LDV mean velocity measurements have $\pm 3.3\%$ relative uncertainty. Turbulence intensity measurements have a relative uncertainty of $\pm 3.4\%$.

III. Experimental Results

A series of tandem cylinder flow control experiments was performed for $22,000 \leq Re_D \leq 172,000$, using both of the experimental configurations shown in Fig. 1. A primary objective of this paper is to compare the efficacy of spanwise and PSVG plasma flow control. In this section of the paper, representative experimental results illustrating their effect for the $Re_D = 22,000$ and $Re_D = 172,000$ cases are presented. It should be noted that the actuator authority (applied voltage) used in the experiments was held constant, independent of Reynolds number. Furthermore, PSVGs are operated only in quasi-steady mode with an unmodulated ac voltage. Hence, both the spanwise and PSVG plasma actuators in the current study were always operated in a quasi-steady mode in the sense that an unmodulated ac carrier of constant frequency was used. No consideration is given to pulsed plasma actuation, as was the case in the single cylinder flow control study reported in [15,16].

A. Global Flow Visualization: $Re_D = 22,000$

In this section, the global effect of plasma flow control on the tandem cylinder flowfield for the lowest Reynolds number case is presented. Figure 4 compares two flow visualization images of the tandem cylinder configuration obtained at $Re_D = 22,000$, both

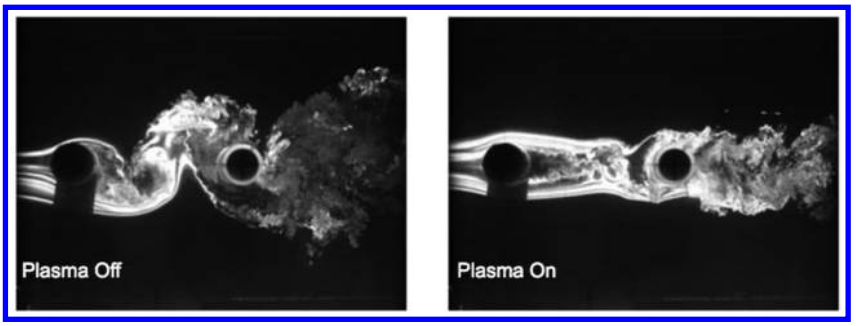

Fig. 4 Flow visualization with and without spanwise plasma actuation at $Re_D = 22,000$.

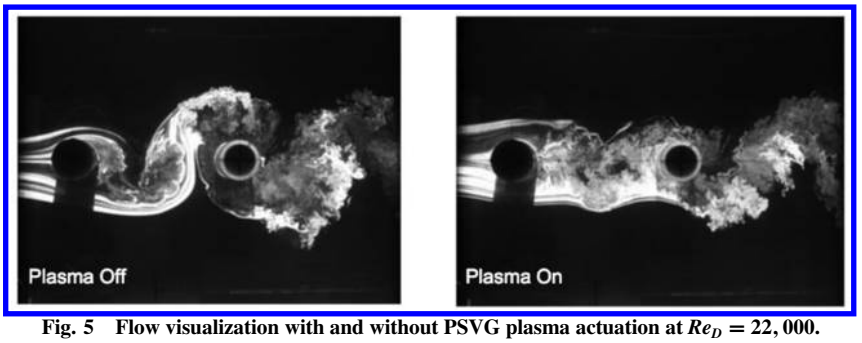

Fig. 5 Flow visualization with and without PSVG plasma actuation at $Re_D = 22,000$.

without and with plasma flow control using the twin spanwise-oriented actuators (i.e., configuration 1 in Fig. 1).

Without plasma flow control, subcritical flow separation from the upstream cylinder occurs and gives rise to large-scale von Kármán vortex shedding. The oscillatory near wake subsequently impinges on the downstream cylinder in an unsteady manner. With plasma flow control, flow separation on the upstream cylinder is considerably delayed and von Kármán shedding is obviously highly suppressed. The upstream cylinder wake is much thinner, and its interaction with the downstream cylinder appears more benign than in the natural case. The plasma actuation causes the flow separation location on the downstream cylinder to shift to the backside.

Figure 5 presents corresponding flow visualization images of the tandem cylinder flow at the same Reynolds number but with and without PSVG plasma actuation applied on the upstream cylinder. In this case, the introduction of streamwise vorticity into the nascent wake shear layers has the effect of considerably delaying flow separation from the upstream cylinder and von Kármán vortex shedding is again suppressed. The wake from the cylinder with PSVG actuation is wider and appears to contain more fine-scale structure than the cylinder wake with spanwise plasma actuation. This suggests higher-turbulence levels and more fine-scale motions in the wake associated with the introduction of streamwise vorticity. Flow separation from the downstream cylinder occurs on the backside.

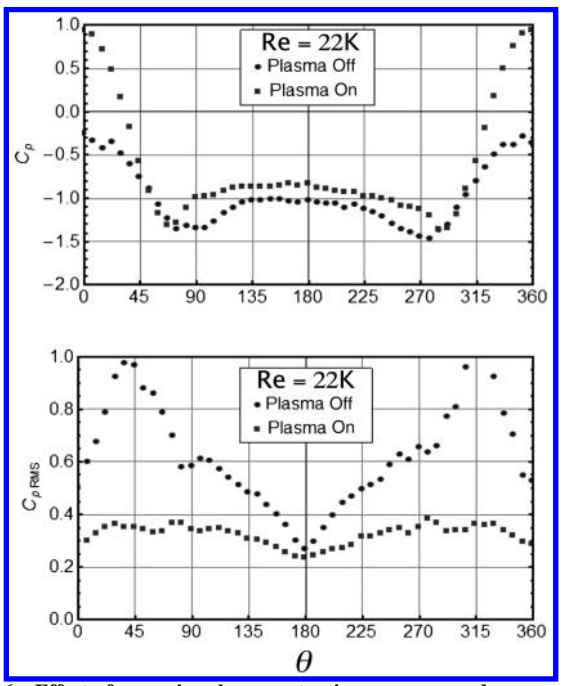

Fig. 6 Effect of spanwise plasma actuation on mean and rms surface pressure distributions.

B. Surface Pressure Measurements: $Re_D = 22,000$

The flush-mounted pressure transducer on the downstream cylinder was used to acquire both mean and rms surface pressure distributions; the unsteady pressure is of particular interest due to its role in the noise generation process. In this section, the influence of both spanwise and PSVG plasma actuation on both mean and unsteady surface pressure on the downstream cylinder is presented.

Figure 6 presents both the mean and rms surface pressures measured for the baseline flow and with spanwise plasma actuation applied on the upstream cylinder. The mean pressure is presented in terms of a pressure coefficient $C_p \equiv 2(P_S - P_\infty)/\rho U_\infty^2$ as a function of azimuthal angle θ (as defined in Fig. 1).

It is apparent that spanwise plasma actuation has a significant effect on the mean pressure distribution on the downstream cylinder. The C_p values are increased from the baseline case, particularly on the windward side of the cylinder for $\theta < 50°$ and $\theta > 310°$. This increase in mean surface pressure is a consequence of suppressed vortex shedding from the upstream cylinder, which results in quasi-steady impingement of the comparatively thin wake on the downstream cylinder front surface, as shown in the flow visualization image of Fig. 4. Figure 6 also presents the rms pressure distribution, $C_{prms} \equiv (\sqrt{\bar{p}_S^2} - P_\infty)/\frac{1}{2}\rho U_\infty^2$, both with and without plasma actuation. For the nonactuated case, peaks in C_{prms} are apparent. The largest, near 40 and 310°, correspond to the unsteady impingement of the wake from the upstream cylinder. The smaller peaks near 98 and 262° correspond to unsteady separation from the downstream cylinder. Figure 6 shows that the application of plasma actuation has a profound effect in reducing unsteady pressure fluctuations on the downstream cylinder. For example, the Cp_{rms} peaks near 40 and

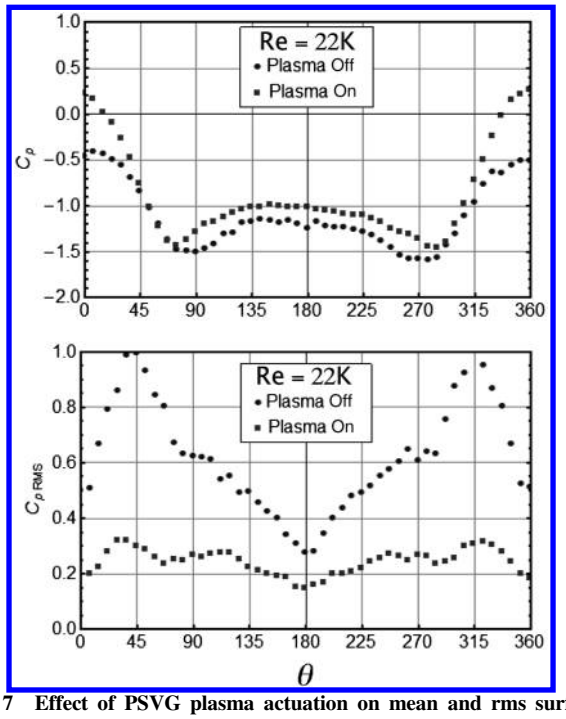

Fig. 7 Effect of PSVG plasma actuation on mean and rms surface pressure distributions.

310° are reduced by approximately 65%. Similarly, the Cp_{rms} peaks near 98 and 262° are reduced by 47%. The 95% relative uncertainty in measured Cp_{rms} is less than ±2.5%.

Figure 7 presents the effect of the PSVG plasma actuation on both mean and rms surface pressure distributions on the downstream cylinder. The mean C_p is again increased on the windward side of the cylinder, but not to the degree achieved with the spanwise plasma actuators. In this case, the effect of the PSVG on the downstream cylinder pressure fluctuations is also significant and Cp_{rms} is again reduced: 68% for the primary rms peaks associated with wake impingement and 62% for the secondary peaks associated with separation on the downstream cylinder.

The power spectral density of surface pressure fluctuations measured on the downstream cylinder at two representative azimuthal locations is presented in Fig. 8 for $Re_D = 22,000$. This figure presents spectra obtained at azimuthal positions, $\theta = 45$ and 105°, for both the natural baseline flow and with spanwise plasma actuation to the upstream cylinder. The measurement at $\theta = 45°$

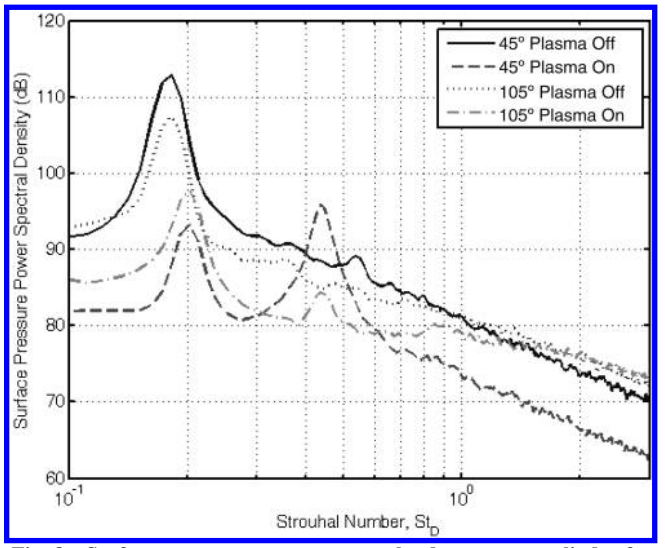

Fig. 8 Surface pressure autospectra on the downstream cylinder for spanwise actuators at $Re_D = 22,000$.

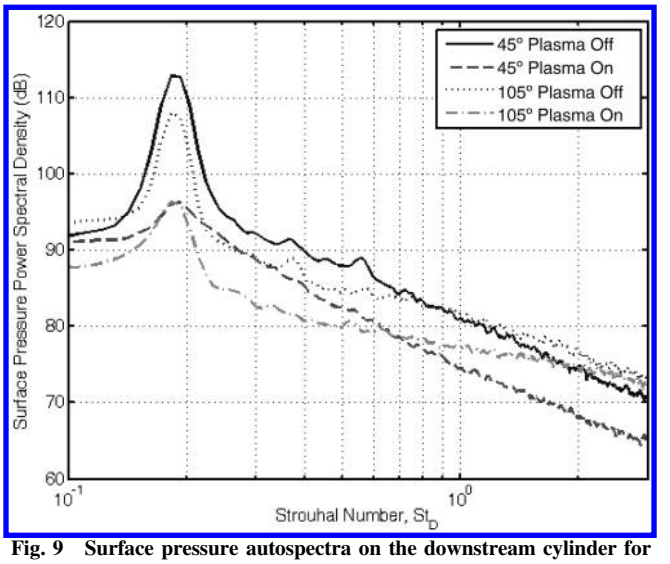

Fig. 9 Surface pressure autospectra on the downstream cylinder for PSVG actuators at $Re_D = 22,000$.

corresponds to a location near impingement of the wake shear layer from the upstream cylinder. The location $\theta = 105°$ is close to the boundary-layer separation point on the rear cylinder. The power spectra are presented in dB with reference to 2×10^{-5} Pa, whereas the frequency is presented in terms of Strouhal number (scaled by the freestream velocity and cylinder diameter). At both azimuthal locations, pressure spectra for the baseline flow case exhibit a strong shedding peak at $St_D = 0.18$ as well as broadband turbulence characteristics. This suggests that shedding from both upstream and downstream cylinders occurs at the same frequency for the baseline flow.

With spanwise plasma actuation turned on, autospectra at both locations exhibit dual peaks at $St_D = 0.2$ and $St_D = 0.44$. It will be shown from wake spectral measurements presented in the next subsection that the peak at $St_D = 0.44$ corresponds to the vortex shedding frequency from the upstream cylinder. This shift to higher shedding frequency is expected based on the plasma-induced reduction in the length scale ℓ of the separated flow on the upstream cylinder. For example, the flow visualization images in Fig. 4 show that the extent of the separated flow region for the baseline case $\ell_{\text{baseline}} \approx \pi R$ and plasma actuation $\ell_{\text{plasma}} \approx \pi R/2$. Assuming that the shedding frequency $f_s \sim U_\infty/\ell$, the change in length scale implies that $f_{s\,\text{plasma}} \approx 2f_{s\,\text{baseline}}$, which is qualitatively consistent with the spectral shift shown in Fig. 8. Comparison of the spectral amplitudes indicates that, in addition to shifting the peak to higher-Strouhal number, the pressure fluctuations associated with wake impingement are reduced by 12.6 dB at $\theta = 45°$. Similarly, there is an 8.3 dB reduction in the spectral peak at the location $\theta = 105°$. Note that the "plasma-on" spectral peak at $St_D = 0.2$ is larger on the rear side of the cylinder ($\theta = 105°$) than on the front side and represents vortex shedding from the downstream cylinder.

Figure 9 compares surface pressure autospectra measured on the downstream cylinder at representative locations $\theta = 45$ and 105°, for both the baseline flow and with PSVG plasma actuation applied to the upstream cylinder. In the case of PSVG plasma actuation, the shedding from the upstream cylinder is effectively suppressed as the spectral peak for $\theta = 45°$ shows an 11.7 dB reduction from the baseline case. Unlike the case with spanwise plasma actuators, there is no significant frequency shift in wake impingement frequency with PSVG plasma actuation. In fact, it is interesting to note that the spectral peak near $St_D = 0.18$ at $\theta = 45°$ for the plasma-on case merges with that at $\theta = 105°$ for the plasma-on case, suggesting that this peak is a manifestation of shedding from the downstream cylinder itself rather than upstream wake impingement. The difference in behavior shown in Fig. 9 is likely due to the character of the shedding from the upstream cylinder with PSVG actuation, which is dominated by small-scale vorticity rather than more organized quasi-two-dimensional vortices. Figure 9 also shows that

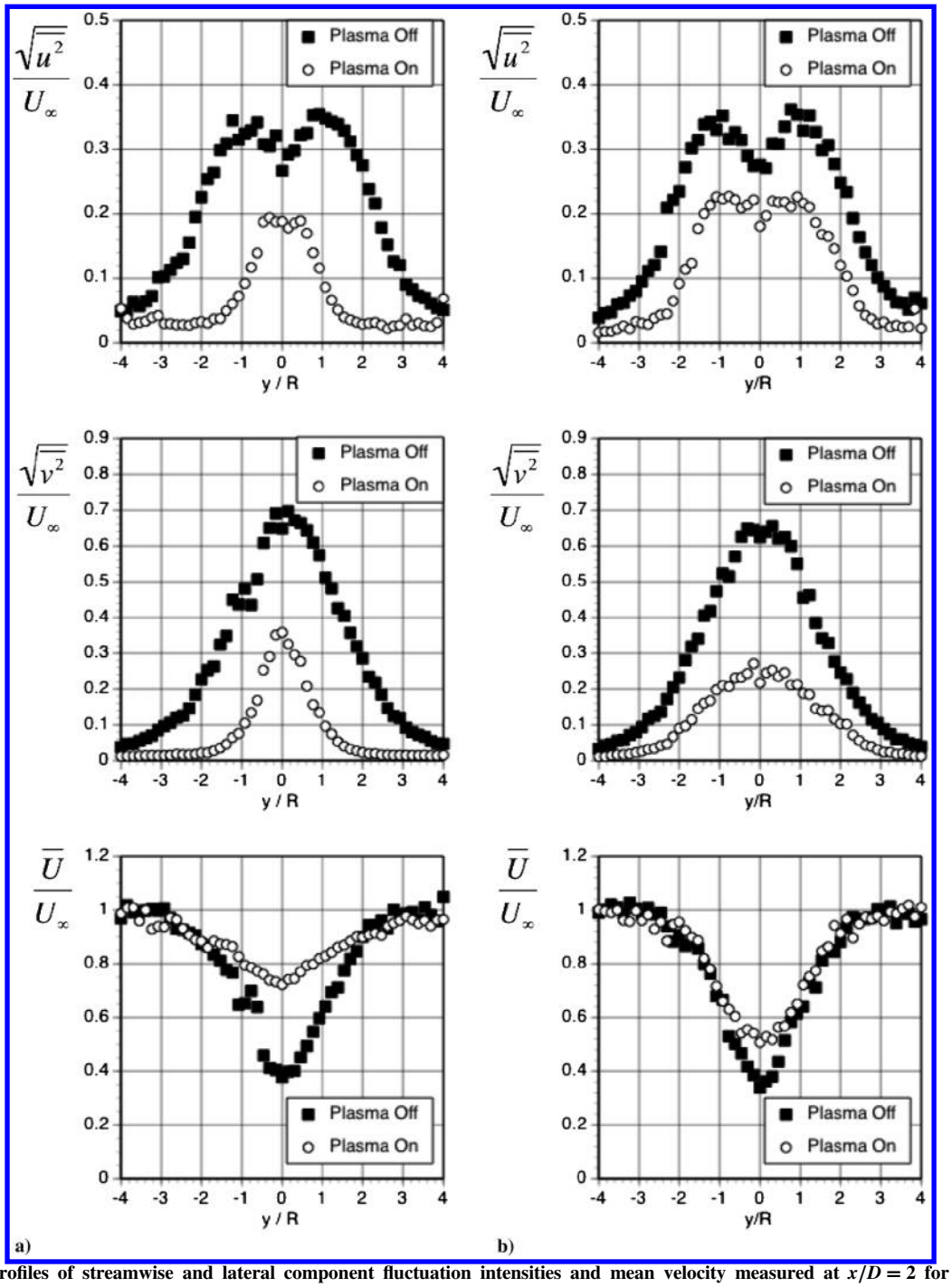

Fig. 10 LDA profiles of streamwise and lateral component fluctuation intensities and mean velocity measured at $x/D = 2$ for $Re_D = 22,000$: (a) spanwise plasma actuators and b) PSVG actuators.

shedding from the second cylinder is also suppressed by approximately 9.1 dB with PSVG plasma flow control.

C. Laser Doppler Anemometry Wake Measurements: $Re_D = 22,000$

In this section, representative LDA cross-stream profiles of mean velocity as well as streamwise and lateral component turbulence intensities and wake autospectra obtained midway between the tandem cylinders are presented. In this manner, the effect of spanwise and PSVG plasma actuation on the upstream cylinder near-wake structure is characterized.

Figure 10 presents representative LDA profiles of turbulence intensity and mean velocity obtained for $Re_D = 22,000$ at $x = 2D$, midway between the two cylinders. Figure 10a compares results for baseline and spanwise plasma actuation. The spanwise actuation reduces the mean velocity wake defect by 54% and the wake width by nearly 60% (based on comparison of fluctuation intensity profiles). Furthermore, the peak level of the streamwise-component turbulence intensity is reduced by 46%, whereas the lateral component intensity is reduced by 49%. It should be noted that the high level of $\sqrt{\overline{v^2}}/U_\infty$ for the baseline case is not due to turbulence per se, but rather is due to the unsteady lateral motion of the near wake resulting from large-scale von Kármán vortex shedding. The large reduction in $\sqrt{\overline{v^2}}/U_\infty$ shown in Fig. 10a is a manifestation of the effective suppression of von Kármán shedding due to the spanwise plasma actuators. It may also be noted that the reduction in wake width that is evident from the LDA profiles in Fig. 10a is consistent with the flow visualization results shown previously in Fig. 4.

Figure 10b presents LDA profiles obtained at the same location ($x = 2D$) and Reynolds number but compares baseline and PSVG plasma actuation cases. It is apparent that the mean velocity wake defect is reduced (24%), as is the wake width (20.4%), with respect to

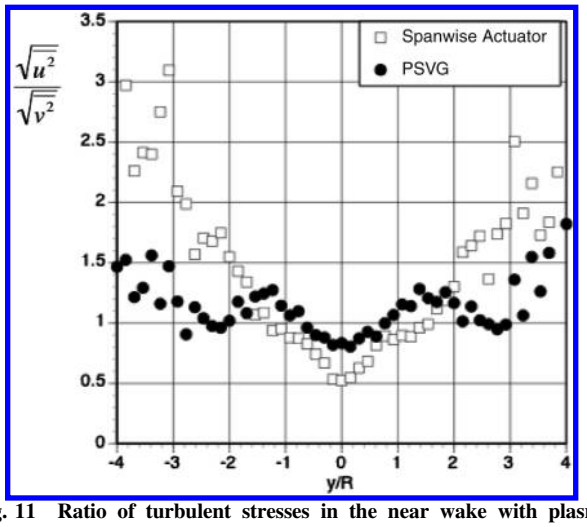

Fig. 11 Ratio of turbulent stresses in the near wake with plasma actuation at $x = 2D$.

the baseline case. However, with PSVG actuation the wake defect is larger and the wake wider than in the case of spanwise plasma actuation shown in Fig. 10a. The larger wake width for the PSVG case relative to spanwise plasma actuation is also apparent from comparison of profiles of $\sqrt{\overline{u^2}}/U_\infty$ and $\sqrt{\overline{v^2}}/U_\infty$ in Figs. 10a and 10b. Nevertheless, Fig. 10b shows a 34% reduction in peak values (relative to baseline) of the streamwise intensity and a 62% reduction in the lateral intensity. This reduction in $\sqrt{\overline{v^2}}/U_\infty$ is considerably larger than with spanwise plasma actuation and is a particularly important metric regarding the reduction of pressure fluctuations on the downstream cylinder.

The flow visualization image with PSVG flow control shown earlier in Fig. 5 suggested enhanced fine-scale motion due to the introduction of streamwise vorticity into the wake. It is of interest to note from Fig. 11 that the profile of the ratio of $\sqrt{\overline{u^2}}/\sqrt{\overline{v^2}}$ with PSVG plasma actuation exhibits relatively small deviation from unity except near the edges of the wake. In comparison, $\sqrt{\overline{u^2}}/\sqrt{\overline{v^2}}$ for the spanwise plasma actuation case deviates more from unity, suggesting a more anisotropic wake structure. The lower values of $\sqrt{\overline{u^2}}/\sqrt{\overline{v^2}}$ for the PSVG case are associated with comparatively fine-scale, three-dimensional wake structure due to the injection of streamwise vorticity into the nascent wake shear layers.

Figure 12 compares v-component wake velocity autospectra obtained via LDA at $x/D = 2$, $y/D = 0$. To perform the spectral analysis using standard FFT methods, the LDA time series were resampled using an interpolation technique. Autospectra for the baseline flow and for the case of spanwise plasma actuation applied on the upstream cylinder are compared. Figure 12 clearly shows both a shift to a much higher shedding Strouhal number ($St_D = 0.18$ to 0.44) and a better than order-of-magnitude reduction in shedding amplitude under the influence of spanwise plasma flow control. This is fully consistent with the interpretation given earlier regarding the shift in surface pressure autospectra peaks to higher St_D on the downstream cylinder when spanwise plasma actuation is applied.

Figure 13 compares v-component velocity autospectra obtained via LDA at $x/D = 2$, $y/D = 0$ for the baseline flow and for the case of PSVG flow control. The comparison reveals a nearly complete suppression of vortex shedding due to the PSVG. Unlike the spanwise plasma actuation case shown in Fig. 12, in which much lower amplitude shedding occurred at higher Strouhal number, Fig. 13 indicates a more complete suppression of large-scale vortex shedding. Evidence for this lies in the broadband nature of the "PSVG on" autospectrum shown in Fig. 13. This full suppression is consistent with surface pressure spectra obtained on the downstream cylinder for PSVG flow control shown in Fig. 9.

D. Global Flow Visualization: $Re_D = 172,000$

In this section, the global effect of plasma flow control on the tandem cylinder flowfield for the highest Reynolds number case is presented. Figure 14 compares flow visualization images for the baseline and spanwise plasma actuation case. The baseline flow case shows vortex shedding from the upstream cylinder and the consequent unsteady interaction of the near wake with the downstream cylinder. Although the Reynolds number is much higher, the behavior is qualitatively similar to that shown in Fig. 4 for the lowest Reynolds number. Figure 14 also shows that when spanwise plasma actuation is applied, flow separation from the upstream cylinder is delayed and von Kármán shedding is clearly suppressed relative to the baseline. The resulting wake is much thinner than for the baseline flow, and its interaction with the downstream cylinder appears much less unsteady in nature. Flow separation from the downstream cylinder is delayed to the backside.

Figure 15 compares baseline and PSVG flow control cases at $Re_D = 172,000$. This figure shows that the PSVG is also effective at the higher Reynolds number at delaying separation from the upstream cylinder and suppressing unsteady von Kármán shedding in the near wake. Although the wake is wider than in the spanwise actuation case, the unsteadiness of the wake interaction with the downstream cylinder appears considerably reduced relative to the baseline case.

E. Surface Pressure Measurements: $Re_D = 172,000$

Figure 16 presents the effect of spanwise plasma actuation on both the mean and rms surface pressure distributions on the downstream cylinder for the $Re_D = 172,000$ case. The mean pressure distribution for the plasma-on case reveals higher-than-baseline

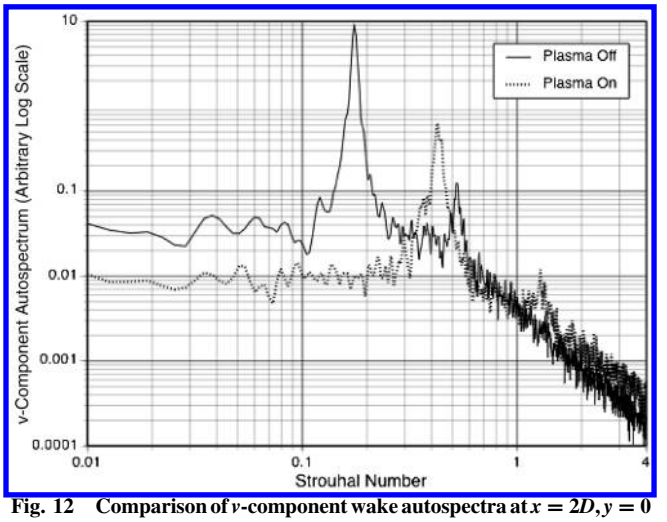

Fig. 12 Comparison of v-component wake autospectra at $x = 2D, y = 0$ with and without spanwise plasma flow control.

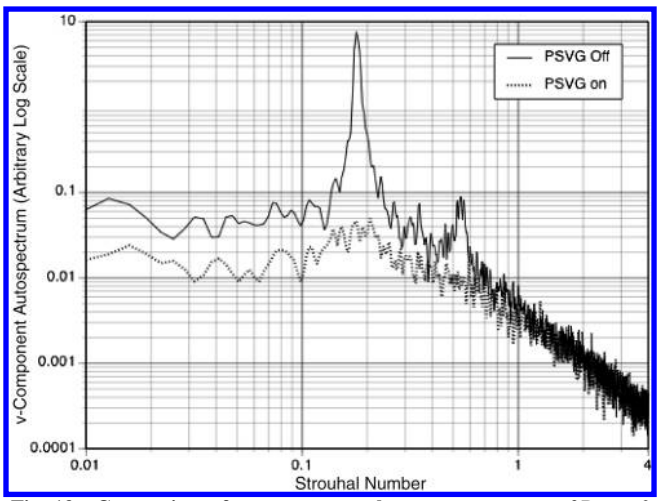

Fig. 13 Comparison of v-component wake autospectra at $x = 2D, y = 0$ with and without PSVG plasma flow control.

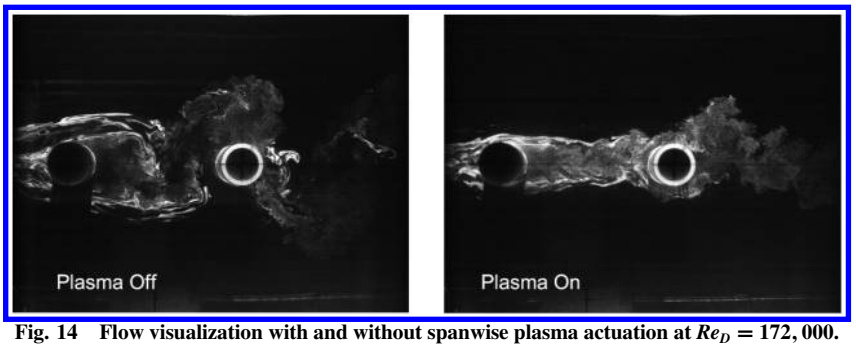

Fig. 14 Flow visualization with and without spanwise plasma actuation at $Re_D = 172,000$.

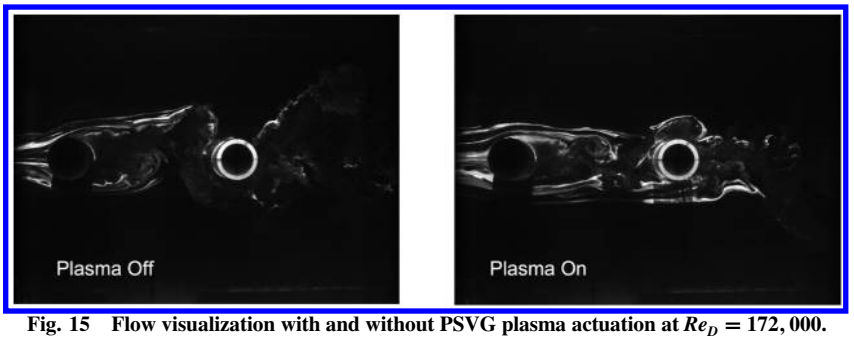

Fig. 15 Flow visualization with and without PSVG plasma actuation at $Re_D = 172,000$.

pressures for $\theta < 45°$ and $\theta > 315°$ and lower pressure for $45° < \theta < 115°$ and $244° < \theta < 318°$. This is consistent with the flow visualization image in Fig. 14, which shows that the spanwise plasma actuation steadies and directs the near wake onto the front surface of the downstream cylinder where the flow attaches and subsequently appears to undergo supercritical separation. Figure 16 also shows that the spanwise plasma actuation has little effect on the base pressure.

Figure 16 indicates that the spanwise plasma actuation provides significant reduction in unsteady pressure on the downstream cylinder. In particular, the C_{prms} peaks near $\theta = 45$ and 315° associated with wake impingement are reduced by 58%, and the peaks associated with flow separation from the downstream cylinder are reduced by 41%. As was the case for spanwise actuation at the lowest Reynolds number, the reduction of unsteady surface pressure shown in Fig. 16 is a direct consequence of suppressing large-scale vortices in the upstream cylinder wake.

Figure 17 compares mean and fluctuating pressure on the downstream cylinder for baseline and PSVG plasma actuation. The effect of the PSVG on the mean pressure is similar to that seen in Fig. 16 for spanwise actuation, but the effect is reduced, i.e., higher-than-baseline pressures for $\theta < 41°$ and $\theta > 322°$ and lower-than-baseline pressure for $41° < \theta < 113°$ and $248° < \theta < 322°$, but to a lesser degree than for spanwise actuation.

Figure 17 shows that the PSVG is able to reduce the unsteady pressure on the downstream cylinder. It should be noted that the baseline rms levels associated with wake impingement are not identical in Figs. 16 and 17, and this is most likely due to the fact that,

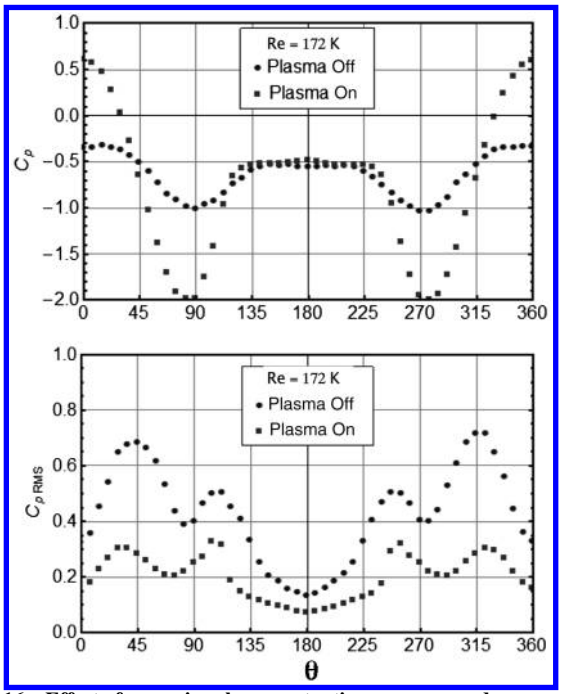

Fig. 16 Effect of spanwise plasma actuation on mean and rms surface pressure distributions.

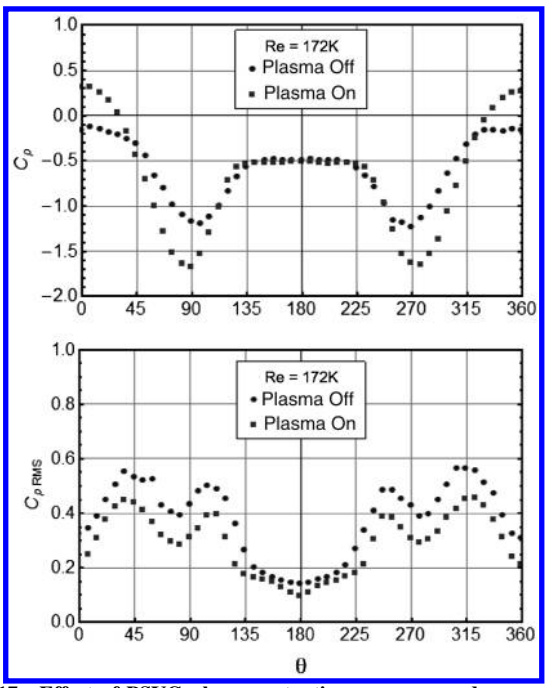

Fig. 17 Effect of PSVG plasma actuation on mean and rms surface pressure distributions.

although the flow at $Re_D = 172,000$ is subcritical, it is very close to the transition to the supercritical state. This makes the cylinder flow at this Reynolds number very sensitive to the small disturbances created by the presence of the 15 PSVG plasma actuators themselves. Nevertheless, the PSVG is found to reduce pressure fluctuations associated with wake impingement by 20.1% (33% relative to the baseline in Fig. 16). Pressure fluctuations associated with separation from the downstream cylinder are reduced by 21% (the same value relative to the baseline in Fig. 16). It is clear that, although the fluctuating pressure is reduced on the downstream cylinder with PSVG flow control, the reductions are not as large as those achieved with spanwise plasma actuation.

Figure 18 compares surface pressure autospectra measured on the downstream cylinder at $\theta = 45$ and 105°, for both the baseline flow and with spanwise plasma actuation at $Re_D = 172,000$. When the plasma actuator is switched on, the shedding frequency changes from $St_D = 0.17$ to a lower amplitude, broad peak centered near $St_D = 0.22 \ldots 0.24$. As was the case at lower Re_D, this shift to higher St_D is associated with a reduction in the characteristic length scale of the separated flow region on the upstream cylinder, which increases the vortex shedding frequency. Despite the increased Reynolds number, integration of the autospectrum reveals that the spanwise plasma actuation reduced the magnitude of the surface pressure fluctuations by 8.3 dB at $\theta = 45°$ and by 6.1 dB at $\theta = 105°$.

Figure 19 compares surface pressure autospectra at $\theta = 45$ and 105°, for both the baseline flow and with PSVG plasma actuation at $Re_D = 172,000$. As was the case for the spanwise plasma flow control, the shedding frequency changes from $St_D = 0.17$ to $St_D = 0.22 \ldots 0.24$ under the influence of PSVG flow control. The complete suppression of shedding by the PSVG demonstrated at $Re_D = 22,000$ does not occur in this case. Integration of the autospectra reveals that the reduction is pressure fluctuations is 1.8 dB at $\theta = 45°$ and by 2.1 dB at $\theta = 105°$. Although this is a significant reduction, it is obviously not as effective as the spanwise actuators.

F. Laser Doppler Anemometry Wake Measurements: $Re_D = 172,000$

In this section, representative cross-stream LDA profiles of mean velocity as well as streamwise and lateral component turbulence intensities obtained midway between the tandem cylinders at $Re_D = 172,000$ are presented.

Figure 20a presents the results of LDA measurements at $x = 2D$, comparing the near wake for baseline and spanwise plasma actuation. As was the case for $Re_D = 22,000$, the spanwise plasma has a very significant effect on the near wake. Peak value of streamwise-component fluctuation intensity is reduced by 22.4%,

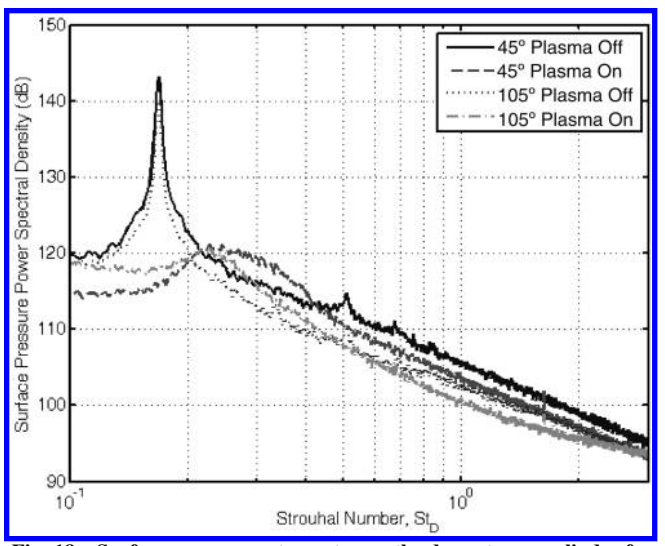

Fig. 18 Surface pressure autospectra on the downstream cylinder for spanwise plasma actuators at $Re_D = 172,000$.

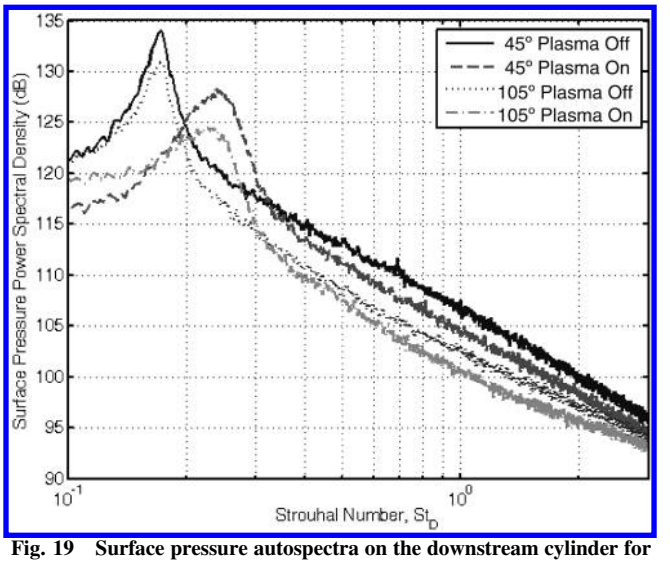

Fig. 19 Surface pressure autospectra on the downstream cylinder for PSVG actuators at $Re_D = 172,000$.

and for the lateral fluctuating component the reduction is 47%. As illustrated in Fig. 14, this is a consequence of suppression of von Kármán vortex shedding from the upstream cylinder by the plasma flow control. Comparison of the baseline and plasma actuated wake mean velocity profiles shown in Fig. 20a shows that the plasma actuation reduces the wake velocity defect by approximately 27%. Both mean and turbulence intensity profiles show that the plasma controlled wake is considerably thinner than in the baseline case. Reduction in wake defect and width is a consequence of the delayed separation on the upstream cylinder due to the twin plasma-induced Coanda wall jets that form on the cylinder surface [15]. Figure 20b presents the results of LDA measurements at $x = 2D$, comparing the near wake for baseline and PSVG plasma actuation. Figure 20b shows that PSVG gives rise to a comparatively modest reduction in $\sqrt{\overline{u^2}}/U_\infty$ of approximately 9.3%. More significantly, the lateral fluctuation intensity $\sqrt{\overline{v^2}}/U_\infty$ is reduced by 43.7%. Unlike the spanwise actuation case, there is little reduction in the wake mean velocity defect by the PSVG, although the wake width is reduced by approximately 12% (as evidenced by the turbulence intensity profiles).

IV. Conclusions

The flow control experiments presented in this study clearly demonstrate that DBD plasma flow control, either in the form of twin spanwise-oriented actuators or PSVG on the upstream cylinder, is quite effective at reducing the rms surface pressure fluctuations on the downstream cylinder of a tandem cylinder arrangement. Although the underlying flow control mechanisms are quite different, both forms of plasma actuation suppress von Kármán vortex shedding from the upstream cylinder, which has the effect of steadying the subsequent wake interaction with the downstream cylinder, thereby reducing surface pressure fluctuations. In the case of spanwise plasma actuation, von Kármán vortex shedding from the upstream cylinder is suppressed by twin plasma-induced wall jets that delay flow separation from the upstream cylinder. The resulting wake is considerably thinner than for the baseline flow, and wake turbulence levels are also greatly reduced. In contrast, the PSVG plasma actuation introduces streamwise vorticity into the nascent wake shear layers and gives rise to a wake with fine-scale vorticity but no large-scale von Kármán vortices. Again, this results in a more benign interaction between the wake and downstream cylinder.

For both spanwise actuation and PSVG, the fundamental physical mechanisms of plasma flow control at $Re_D = 22,000$ and 172,000 appear quite similar. At the lowest Reynolds number, both spanwise plasma actuation and PSVG appear equally effective. However, the spanwise actuators are shown to provide a larger reduction in surface

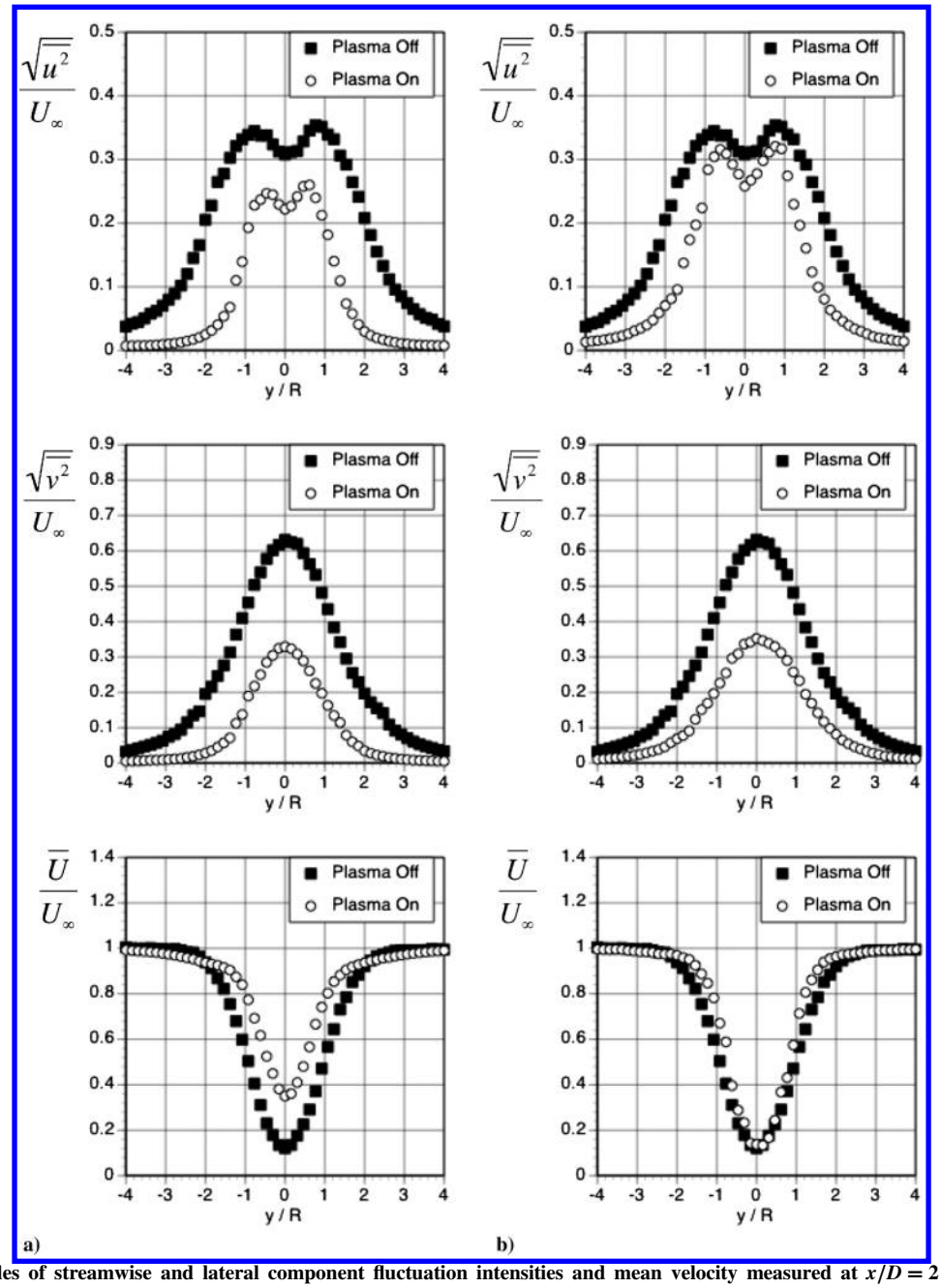

Fig. 20 LDA profiles of streamwise and lateral component fluctuation intensities and mean velocity measured at $x/D = 2$ for $Re_D = 172,000$: a) spanwise plasma actuators and b) PSVG actuators.

pressure fluctuations at the largest Reynolds number. Caution should be used in concluding that spanwise plasma actuation is the preferred mode of flow control at high subcritical Reynolds numbers, however, because no effort was made to adjust either the spanwise electrode spacing or the PSVG actuator authority with increasing Re_D. It is noted that in numerical simulations of single cylinder flow control at $Re_D = 100$ using distributed spanwise sinusoidal blowing, Kim and Choi [24] found a preferred spanwise wavelength of 4–5D. Although not directly relevant because the Reynolds number is quite low and the form of flow control is different than PSVG, it does suggest the possibility of a preferred spanwise wavelength for PSVG; this aspect is beyond the scope of the present study.

Finally, it is conjectured that for cylinders at supercritical Reynolds numbers both forms of plasma flow control should also be quite effective because suppression of shedding is actually more difficult in the subcritical regime. For supercritical flow, the separation location shifts to the backside of the cylinder due to the boundary-layer transition to turbulence. Hence, it may be useful to position the spanwise actuators on the backside of the cylinder at a location just upstream of the supercritical flow separation. In addition, there would also likely be a benefit gleaned by lengthening the streamwise electrodes for the PSVG such that they extend over a portion of the rear cylinder surface. It is also conjectured that the actuation authority required for effective plasma flow control at supercritical Reynolds numbers would be comparable to that used in the current study.

Acknowledgment

This work was supported by NASA through Cooperative Agreement no. NNX07AO09A, which was monitored by Clif Horne and William Humphreys. This support is gratefully acknowledged.

References

[1] Jenkins, L. N., Khorrami, M. R., Choudhari, M. M., and McGinley, C. B., "Characterization of Unsteady Flow Structure Around Tandem Cylinders for Component Interaction Studies in Airframe Noise," AIAA Paper 2005-2812, 11th AIAA/CEAS Aeroacoustics Conference,

Monterey, CA, 23–25 May 2005.
[2] Jenkins, L. N., Neuhart, D. H., McGinley, C. B., Choudhari, M. M., and Khorrami, M. R., "Measurements of Unsteady Wake Interference Between Tandem Cylinders," AIAA Paper 2006-3202, 36th AIAA Fluid Dynamics Conference, San Francisco, CA, 5–8 June 2006.
[3] Khorrami, M. R., Choudhari, M. M., Jenkins, L. N., and McGinley, C. B., "Unsteady Flowfield Around Tandem Cylinders as Prototype for Component Interaction in Airframe Noise," AIAA Paper 2005-2866, 11th AIAA/CEAS Aeroacoustics Conference, Monterey, CA, 23–25 May 2005.
[4] Neuhart, D. H., Jenkins, L. N., Choudhari, M. M., and Khorrami, M., "Measurements of the Flowfield Interaction Between Tandem Cylinders," 15th AIAA/CEAS Aeroacoustics Conference, AIAA Paper 2009-3275, Miami, FL, May 2009.
[5] Hutcheson, F., and Brooks, T., "Noise Radiation from Single and Multiple Rod Configurations," AIAA Paper 2006-2629, 2006.
[6] Thomas, F. O., Kozlov, A. V., ELTaweel, A., Wang, M., and Kim, D., "Plasma Flow Control in a Tandem Cylinder Configuration: Experiment and Large-Eddy Simulation," 16th AIAA/CEAS Aeroacoustics Conference, AIAA Paper 2010-3790, Stockholm, May 2010.
[7] Lockard, D. P., Choudhari, M. M., Khorrami, M. R., Neuhart, D. H., Hutcheson, F. V., and Brooks, T. F., "Aeroacoustic Simulations of Tandem Cylinders with Subcritical Spacing," AIAA Paper 2008-2862, 2008.
[8] Tinetti, A. F., and Dunn, M. H., "Acoustic Simulations of an Installed Tandem Cylinder Configuration," 15th AIAA/CEAS Aeroacoustics Conference, AIAA Paper 2009-3158, Miami, FL, May 2009.
[9] Frendi, A., and Yuzhi, Sun, "Noise Radiation from Two Circular Cylinders in Tandem Arrangement Using High-Order Multidomain Spectral Difference Method," 15th AIAA/CEAS Aeroacoustics Conference, AIAA Paper 2009-3159, Miami, FL, May 2009.
[10] Doolan, C. J., "Flow and Noise Simulation of the NASA Tandem Cylinder Experiment Using OpenFOAM," 15th AIAA/CEAS Aeroacoustics Conference, AIAA Paper 2009-3157, Miami, FL, May 2009.
[11] Zdravkovich, M. M., "Flow Induced Oscillations of Two Interfering Circular Cylinders," *Journal of Sound and Vibration*, Vol. 101, No. 4, 1985, pp. 511–521.
doi:10.1016/S0022-460X(85)80068-7
[12] Arie, M., Kiya, M., Moriya, M., and Mori, H., "Pressure Fluctuations on the Surface of Two Circular Cylinders in Tandem Arrangement," *Journal of Fluids Engineering*, Vol. 105, June 1983, pp. 161–167.
doi:10.1115/1.3240956
[13] Gu, Z., "On Interference Between Two Circular Cylinders at Supercritical Reynolds Number," *Journal of Wind Engineering and Industrial Aerodynamics*, Vol. 62, Nos. 2–3, 1996, pp. 175–190.
doi:10.1016/S0167-6105(96)00056-6
[14] Thomas, F. O., Kozlov, A., and Corke, T. C., "Plasma Actuators for Landing Gear Noise Control," 11th AIAA/CEAS Aeroacoustics Conference, AIAA Paper 2005-3010, 2005.
[15] Thomas, F. O., Kozlov, A., and Corke, T. C., "Plasma Actuators for Cylinder Flow Control and Noise Reduction," *AIAA Journal*, Vol. 46, No. 8, 2008, pp. 1921–1931.
doi:10.2514/1.27821
[16] Thomas, F. O., Kozlov, A., and Corke, T. C., "Plasma Actuators for Bluff Body Flow Control," AIAA Paper 2006-2845, 2006.
[17] Kozlov, A., and Thomas, F. O., "Active Control of Bluff Body Flows Using Dielectric Barrier Discharge Plasma Actuators," 15thAIAA/CEAS Aeroacoustics Conference, AIAA Paper 2009-3245, Miami, FL, 2009.
[18] Kim, D., and Wang, M., "Large-Eddy Simulation of Flow Over a Circular Cylinder with Plasma-Based Control," AIAA Paper 2009-1080, 2009.
[19] Corke, T. C., Post, M. L., and Orlov, D. M., "Single Dielectric Barrier Discharge Plasma Enhanced Aerodynamics: Physics, Modeling and Application," *Experiments in Fluids*, Vol. 46, No. 1, 2009, pp. 1–26.
doi:10.1007/s00348-008-0582-5
[20] Moreau, E., "Airflow Control by Non-Thermal Plasma Actuators," *Journal of Physics D Applied Physics*, Vol. 40, No. 3, 2007, pp. 605–636.
doi:10.1088/0022-3727/40/3/S01
[21] Dowling, A. P., and Ffowcs Wiliams, J. E., *Sound and Sources of Sound*, Ellis Horwood, London, 1983, pp. 163–166.
[22] Schatzman, D. M., and Thomas, F. O., "Turbulent Boundary Layer Separation Control with Single Dielectric Barrier Discharge Plasma Actuators," *AIAA Journal*, Vol. 48, No. 8, 2010, pp. 1620–1634.
doi:10.2514/1.J050009
[23] Thomas, F. O., Corke, T. C., Iqbal, M., Kozlov, A., and Schatzman, D., "Optimization of SDBD Plasma Actuators for Aerodynamic Flow Control," *AIAA Journal*, Vol. 47, No. 9, 2009, pp. 2169–2178.
doi:10.2514/1.41588
[24] Kim, J., and Choi, H., "Distributed Forcing of Flow over a Circular Cylinder," *Physics of Fluids*, Vol. 17, No. 3, 2005, pp. 033103.
doi:10.1063/1.1850151

T. Jackson
Associate Editor